Exploration of Anti-Diabetic Potential of Rubus ellipticus Smith through Molecular Docking, Molecular Dynamics Simulation, and MMPBSA Calculation

P. Neupane, S. Dhital, N. Parajuli, T. Shrestha, S. Bharati, B. Maharjan, J. Adhikari Subin, R. L. S. Shrestha

Journal of Nepal Physical Society

Volume 9, Issue 2, December 2023

ISSN: 2392-473X (Print), 2738-9537 (Online)

JNPS, **9** (2): 95-105 (2023)

DOI: https://doi.org/10.3126/jnphyssoc.v9i2.62410

Published by:

Nepal Physical Society
P.O. Box: 2934
Tri-Chandra Campus
Kathmandu, Nepal
Email: nps.editor@gmail.com

JNPS 9 (2): 95-105 (2023)
ISSN: 2392-473X (Print), 2738-9537 (Online)

Research Article *© Nepal Physical Society*
DOI: https://doi.org/10.3126/jnphyssoc.v9i2.62410

Exploration of Anti-Diabetic Potential of *Rubus ellipticus* Smith through Molecular Docking, Molecular Dynamics Simulation, and MMPBSA Calculation

P. Neupane[1], S. Dhital[1], N. Parajuli[1], T. Shrestha[1], S. Bharati[1], B. Maharjan[1], J. Adhikari Subin[2, *], R. L. S. Shrestha[1, 3, *]

[1]Department of Chemistry, Amrit Campus, Tribhuvan University, Thamel, Kathmandu 44600, Nepal

[2]Bioinformatics and Cheminformatics Division, Scientific Research and Training Nepal P. Ltd., Kaushaltar, Bhaktapur 44800, Nepal

[3]Institute of Natural Resources Innovation, Kalimati, Kathmandu 44600, Nepal

Corresponding Email: subinadhikari2018@gmail.com, swagatstha@gmail.com

Received: *22nd June, 2023;* ***Revised:*** *16th December, 2023;* ***Accepted:*** *29th December, 2023*

ABSTRACT

Diabetes is a chronic metabolic disorder affecting a majority of the population worldwide. Hyperglycemia leading to diabetes mellitus could be managed through the inhibition of human pancreatic α-amylase enzyme. Phytochemicals are frequently reported to possess anti-diabetic activity through inhibition of normal functioning of α-amylase. This study aims to find potential α-amylase inhibitors from *Rubus ellipticus* Smith. with molecular-level understanding using different computational tools. From the molecular docking calculations, rubuside F and rubuside D possessed good binding affinity of -10.0 kcal/mol and -9.9 kcal/mol, respectively better than that of the reference drugs (acarbose, miglitol, voglibose, and metformin). Both the compounds showed good geometrical stability from molecular dynamics simulation accessed in terms of RMSD, hydrogen bond count, SASA, R_g and RMSF. Binding free energy changes of -27.92±4.15 kcal/mol and -28.75±4.15 kcal/mol, respectively for the two ligands indicated sustained thermodynamic spontaneity present in the adducts. The two phytochemicals could be proposed as potential inhibitors of human pancreatic α-amylase for the treatment of diabetes. Further, *in vitro* and *in vivo* experiments are recommended for the verification of computational insights in the course of drug design and discovery process.

Keywords: α-amylase, Binding affinity, Computational, Hyperglycemia.

INTRODUCTION

The use of herbal remedies to treat various illnesses dates back to ancient times and is still widely practised [1]. Medicinal plants contain naturally occurring active components used to treat illness or to alleviate pains [2]. The antioxidant, antibacterial, and antipyretic activities of the phytochemicals found in plants could be the root of their therapeutic qualities [3]. Through several metabolic processes, the plant creates a range of secondary metabolites crucial for boosting the immune system and treating diseases [4]. According to the World Health Organization, medicinal plants are an ideal source of a broad spectrum of medication with 80% of the developing world still benefiting from it [5].

Rubus ellipticus Smith., a thorny shrub belonging to family Rosaceae is widely distributed in the forest of Nepal [6]. It is commonly known as the yellow himalayan raspberry [7] and is found in sparse forests, montane valleys, and roadsides at the height of 300 - 2600 m [8]. The Rubus species has been employed in traditional medicine due to its valuable pharmacological and ethnomedicinal characteristics [6]. Various components of the plant have been reported to possess therapeutic value in treating conditions such as diarrhea, epilepsy and dysentery,

and also function as an antimicrobial, wound healing agent, analgesic, anti-fertility agent, and a renal tonic [9]. In ancient folk medicine, the plant has been employed for the treatment of diabetes, and numerous studies show its effectiveness in diabetes management [9–12].

Diabetes mellitus is a chronic metabolic condition resulting from hyperglycemia linked to inadequate insulin production or insulin resistance in cells [13]. According to IDF Diabetes Atlas (2021), 540 million people worldwide currently possesses diabetes, and the number is anticipated to increase by 46% by 2045 [14]. Moreover, currently, 10.5% of the adult population is suffering from diabetes, with almost half of them unaware of their medical condition [14]. Among the several digestive enzymes, human pancreatic α-amylase (HPAA) is the most significant as it catalyzes the hydrolysis of α-1,4 glycosidic linkage in starch, amylopectin, glycogen, and several maltodextrins [13,15]. During the hydrolysis of starch, an amino acid residue of catalytic triad ASP197 functions as a nucleophile, while GLU233 and ASP300 function as acid/base catalysts [16].

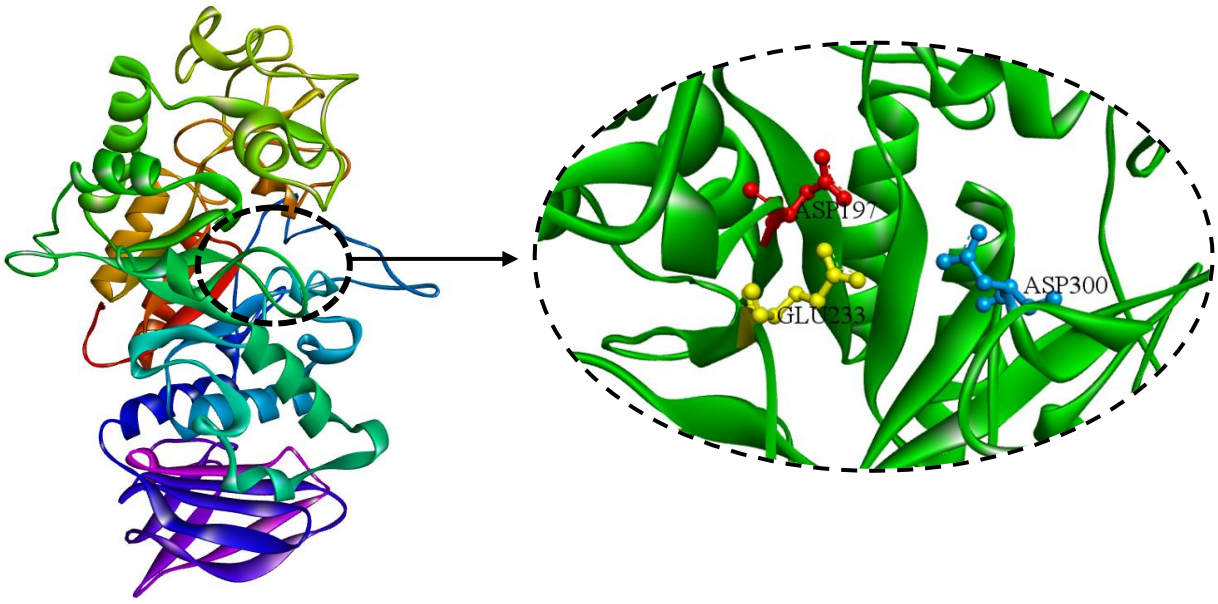

Fi. 1: Catalytic triad (ASP197, GLU233, and ASP300 as ball-and-stick model) of the binding pocket of α-amylase.

One of the treatment strategies for managing diabetes is the inhibition of α-amylase [13]. Acarbose, miglitol, and voglibose are commonly used α-amylase inhibitors, nevertheless, they come with several adverse effects, including bloating, diarrhoea, and stomach pain [17]. Since managing the disease without any side effects remains somewhat challenging, plants continue to be vital in exploring safe novel molecules to treat diabetes [18].

The drug development process has steadily adopted synergistic experimental and computational approaches in recent years since they are effective and economical [19]. This study combines molecular docking, molecular dynamics simulation (MDS) and binding free energy calculations to determine the most stable docked ligand capable of inhibiting the receptor protein. The objective of this computational investigation is to determine the potential inhibitors of α-amylase from a set of compounds derived from a literature review that were isolated from *Rubus ellipticus* Smith. for therapeutics against diabetes.

MATERIALS AND METHODS

Selection and preparation of ligands

The ligands were selected from the literature review of isolated compounds of *Rubus ellipticus* [20–23]. ChemDraw software was employed to sketch 2D structures of the ligands, which were subsequently transformed into 3D structures and saved in pdb format [24]. The pdb format was converted using AutoDock Tools to pdbqt format by the addition of Gasteiger charge [25]. Utilizing the Avogadro program, structural minimization of the ligands was performed [26]. Universal force field (UFF) was selected and the geometry optimization was done up to 2000 number of steps following conjugate gradient algorithm.

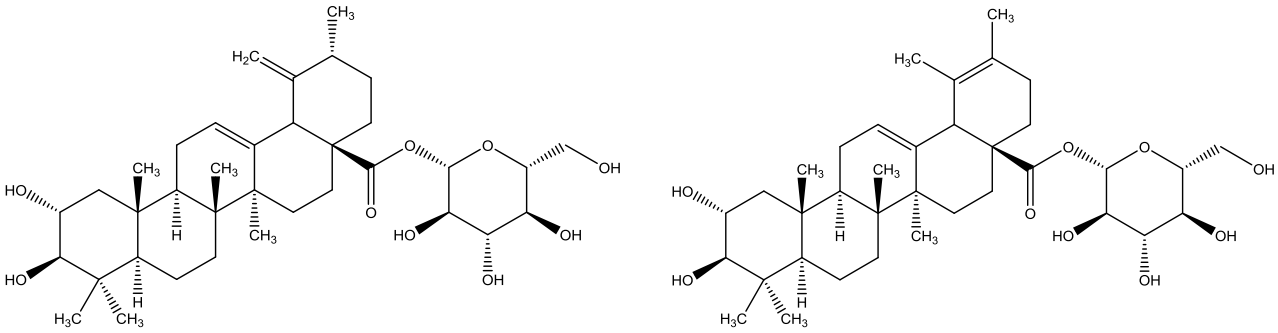

Rubuside F **Rubuside D**

Fig. 2: Chemical structures of two representative ligands of *R. ellipticus.*

Target selection and preparation

The high-resolution crystalline protein structure of human pancreatic α-amylase enzyme (PDB ID: 2QV4) of 1.97 *Å* resolution was obtained from the RCSB database [27]. Visualization of the protein structure was accomplished using the PyMOL program [28]. The protein was cleaned, polar hydrogens were added, and the molecule was saved in pdb format using PyMOL. Autodock Vina was utilized to incorporate polar hydrogen and Kollman charge into the protein structure, and it was subsequently converted to the pdbqt format required for molecular docking.

Molecular docking calculations

Molecular docking is used to anticipate the plausible conformations and orientations of the ligand within the orthosteric pocket of the target protein, as well as to estimate the binding affinity of the complex [29]. Molecular docking was carried out using Autodock Vina software, where the ligands were flexible and the protein remained rigid [25]. The number of poses of 20, an energy range of 4 units, and an exhaustiveness of 32 were chosen for the docking process. The identification of the best protein-ligand complex were done on the basis of binding affinity (kcal/mol) of each complex. Subsequently, 2D and 3D visualization of protein-ligand interactions were done using the Biovia Discovery Studio [30] and Chimera programs [31]. For interpretation, further investigation, and molecular dynamics simulation, the pose with the most favorable binding energy was chosen. The center of the receptor's grid box was set at (14.029, 49.559, and 20.381) within the protein's active site, with a grid box size of 38×40×38 $Å^3$ and a spacing of 0.375 *Å*. The docking protocol validation was done through superimposition of native ligand in the protein crystal with the docked ligand, resulting in a good RMSD of 1.3 *Å* [32].

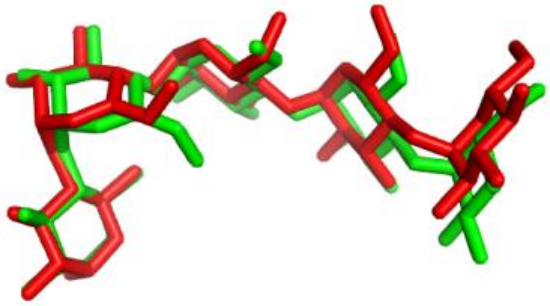

Fig. 3: Superimposition of native ligand in crystalline structure (red) with native ligand in docked structure (green).

Molecular Dynamics Simulation

Molecular dynamics simulations (MDS) of the protein-ligand complexes were executed using the GROMACS program [33], employing the Charmm27 force field [34] obtained from the SwissParam server [35] for both the ligand and the receptor. The system was solvated in a triclinic box using the TIP3P water model with a spacing of 10 *Å*. The system was neutralized with an isotonic NaCl solution. Equilibration of the system at a physiological temperature of 310 K was achieved through four stages, two NVT equilibrium (500 ps and 600 ps) and two NPT equilibrium (500 ps each). The subsequent production run spanned 100 ns without constraints, and various parameters, including radius of gyration (R_g), root mean square deviation (RMSD), number of hydrogen bonds, solvent-accessible surface area (SASA), and root mean square fluctuation (RMSF) were extracted from the trajectory using built-in modules. The RMSD trajectory obtained from the MD simulation served as the basis for assessing the stability of the protein-ligand adduct during the projection run.

Binding free energy change estimation

The MMPBSA method, employing the Poisson Boltzmann solvation model was utilized to compute

the change in binding free energy of the complex [36]. Through the free energy changes, an evaluation of the spontaneity and feasibility of the forward reaction was done. This calculation was performed on the equilibrated portion (20 ns) of the MDS trajectory.

The binding free energy is given by the equation [37]:

$\Delta G_{Bind} = \Delta G_{complex} - \Delta G_{protein} - \Delta G_{ligand}$ ---------- (1)

and can be decomposed as equation (2)

$\Delta G_{BFE} = \Delta G_{VDW} + \Delta G_{EL} + \Delta G_{PB} + \Delta G_{SURF} - T\Delta S$ --- (2)

$\Delta G_{BFE} = \Delta G_{Gas} + \Delta G_{Solvent} - T\Delta S$ ---------- (3)

The consideration of the conformational entropy term (−TΔS) was omitted because of the significant computational cost and technical errors associated with its calculation [37].

RESULTS AND DISCUSSION

Docking scores

The binding affinity obtained from molecular docking relies on various factors such as the polarity of ligands, the flexibility of molecules, molecular weight of ligands, and the size of the binding pocket [38, 39]. Docking relies on two key components: search algorithms, which analyze and generate ligand poses at a target's binding site, and scoring functions that rank the poses and orientation of ligands based on binding affinity [40]. From the molecular docking, it was evident that most ligands showed better binding affinity than all the reference drugs (acarbose, miglitol, voglibose, and metformin) as shown in Table 1. But neither of the docked compounds demonstrated binding affinity greater than the native ligand with -10.4 kcal/mol. However, among the docked compounds, rubuside D exhibited comparative binding affinity of -10.0 kcal/mol with the native ligand. Similarly, good binding affinities of -9.9 kcal/mol, -9.6 kcal/mol, and -9.6 kcal/mol were observed with rubuside F, sericoside and rosamutin respectively. The binding affinities indicated that the ligands were docked strongly with proper orientation at the active site. Thus, the compounds of *Rubus ellipticus* could possibly inhibit the normal functioning of the human pancreatic α-amylase.

Table 1: Binding affinities of ligands of *Rubus ellipticus* and drugs with human pancreatic a-amylase

S.N.	Ligands	Binding affinity (kcal/mol)	S.N.	Ligands	Binding affinity (kcal/mol)
1	Rubuside D	-10.0	13	Nigaichigoside F1	-9.1
2	Rubuside F	-9.9	14	Rubuside I	-9.1
3	Sericoside	-9.6	15	Rubuside J	-9.0
4	Rosamutin	-9.6	16	Rubuside H	-8.9
5	Rubuside A	-9.5	17	Buergericic acid	-8.5
6	Rubuside E	-9.5	18	Sericic acid	-8.3
7	Pinfaensin	-9.4	19	Acarbose	-7.6
8	Kajiichigoside F1	-9.4	20	Voglibose	-6.1
9	Rubuside B	-9.4	21	Miglitol	-5.8
10	Alpinoside	-9.1	22	Metformin	-5.4
11	Quadranoside VIII	-9.1	23	Native	-10.4
12	Rubuside G	-9.1			

Protein-ligand interactions

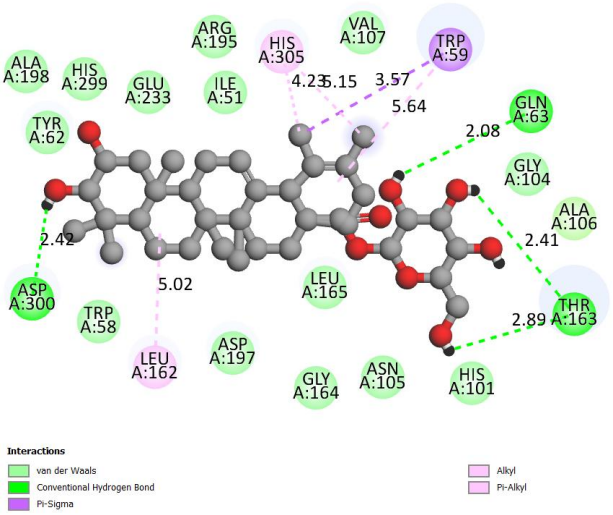

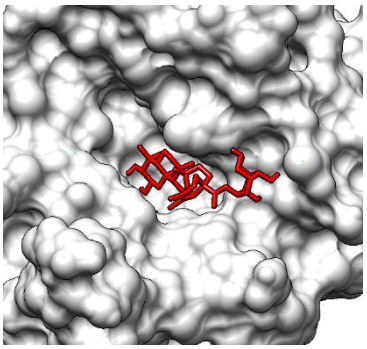

Rubuside D

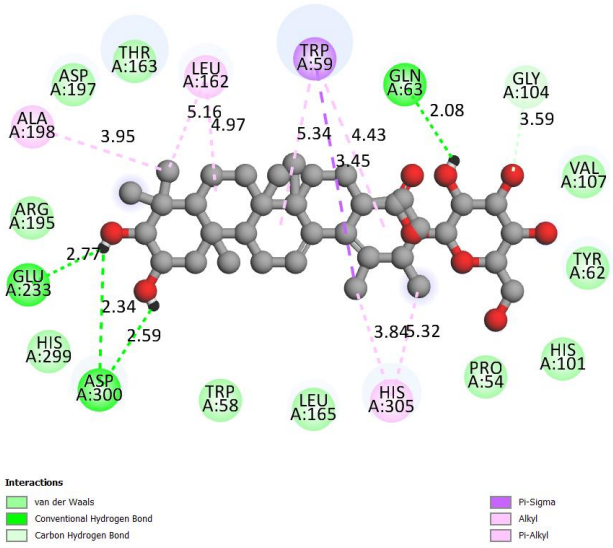

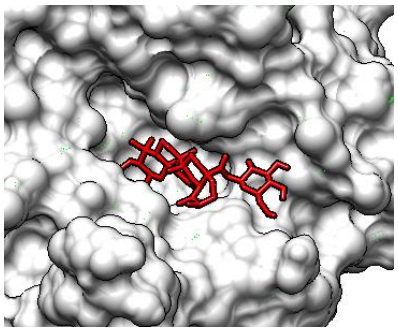

Rubuside F

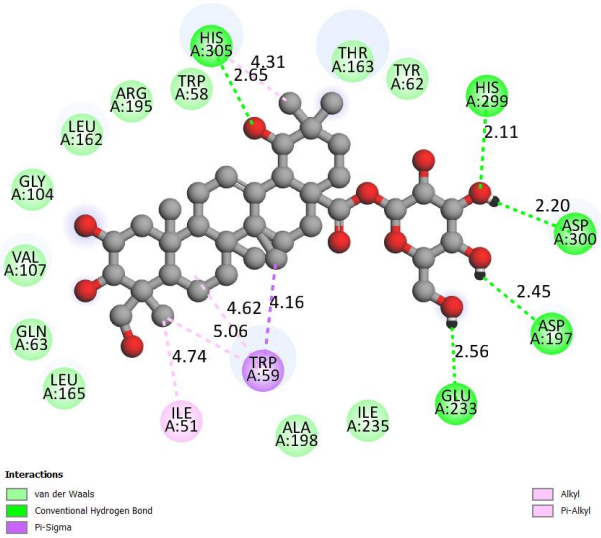

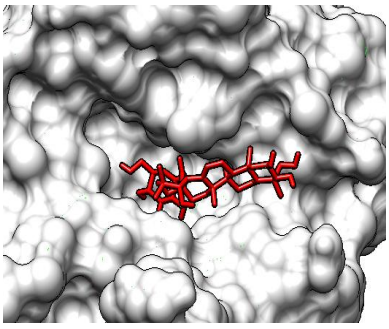

Sericoside

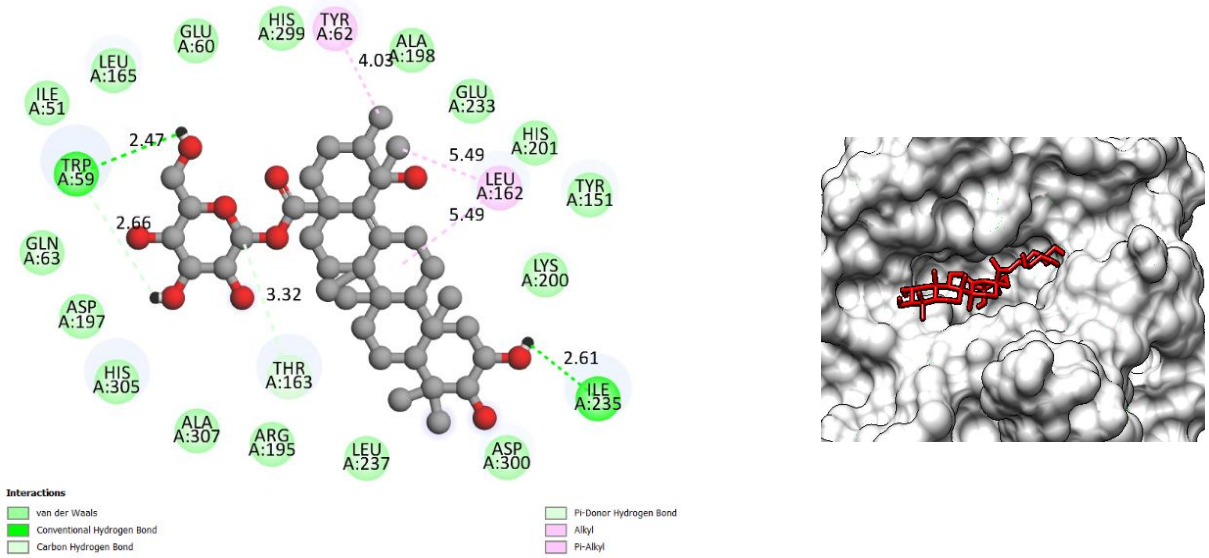

Rosamutin

Fig. 4: 2D interaction (left) and 3D docked ligand at the binding pocket (right) of top four ligands with human pancreatic α-amylase (PDB ID: 2QV4)

The best four protein-ligand adducts with the interactions are depicted in Figure 4. The ligands interacted with the amino acid of the protein forming several hydrophilic and hydrophobic bonds. Among the interactions, hydrophilic interactions were mostly observed between the ligand and the protein. Several hydrogen bonds were formed between the ligand and the amino acid residue with the highest five hydrogen bonds with sericoside and the lowest two hydrogen bonds with rosamutin. The majority of ligands interacted with the catalytic triad: **ASP197**, **GLU233** and **ASP300** forming stronger hydrogen bonds (2.20 *Å* to 2.77 *Å*). Moreover, the distance of the hydrogen bond ranged from 2.08 *Å* to 2.77 *Å* indicating stronger binding of the ligands at the orthosteric site. Some of the ligands, namely rubuside F and rosamutin interacted with Pi-donor hydrogen bonds and carbon-hydrogen bonds. In addition to the hydrogen bonds, several hydrophobic interactions such as alkyl, Pi-alkyl, and Pi-sigma interaction were observed. Numerous van der Waals interactions were formed between the ligands and the amino acid residue of the protein. The interactions between the top four ligands with the amino acid residues inferred that the ligands formed stronger hydrogen bonds with the catalytic triad along with other favorable interactions and thus could inhibit the normal functioning of human pancreatic α-amylase.

Table 2: Interactions of top four ligands with different amino acid residues of α-amylase

Ligands	Binding affinity (Kcal/mol)	Types of interactions	Active site residues (Distance Å)
Rubuside D	**-10.0**	Hydrogen Bond	GLN63 (2.08), THR163 (2.41, 2.89), **ASP300** (2.42)
		Pi-Sigma	TRP59 (3.57)
		Pi-Alkyl	TRP59 (5.64), HIS305 (4.23, 5.15)
		Alkyl	LEU162 (5.02)
		van der Waals	ILE51, TRP58, TYR62, HIS101, GLY104, ASN105, ALA106, VAL107, GLY164, LEU165, ARG195, **ASP197**, ALA198, **GLU233**, HIS299
		Hydrogen Bond	GLN63 (2.08), **GLU233** (2.77), **ASP300** (2.34, 2.59)

Rubuside F	**-9.9**	Carbon-hydrogen bond	GLY104 (3.59)
		Pi-Sigma	TRP59 (3.45)
		Alkyl	LEU162 (4.97, 5.16), ALA198 (3.95)
		Pi-Alkyl	TRP59 (4.43, 5.34), HIS305 (3.84, 5.32)
		van der Waals	PRO54, TRP58, TYR62, HIS101, VAL107, THR163, LEU165, ARG195, **ASP197**, HIS299
Sericoside	**-9.6**	Hydrogen Bond	**ASP197** (2.45), **GLU233** (2.56), HIS299 (2.11), **ASP300** (2.20), HIS305 (2.65)
		Pi-Sigma	TRP59 (4.16)
		Alkyl	ILE51 (4.74)
		Pi-Alkyl	TRP59 (4.62, 5.06), HIS305 (4.31)
		van der Waals	TRP58, TYR62, GLN63, GLY104, VAL107, LEU162, THR163, LEU165, ARG195, ALA198, ILE235
Rosamutin	**-9.6**	Hydrogen Bond	TRP59 (2.47), ILE235 (2.61)
		Carbon-hydrogen bond	THR163 (3.32)
		Pi-Donor Hydrogen bond	TRP59 (2.66)
		Alkyl	LEU162 (5.49, 5.49)
		Pi-Alkyl	TYR62 (4.03)
		van der Waals	ILE51, GLU60, GLN63, TYR151, LEU165, ARG195, **ASP197**, ALA198, LYS200, HIS201, **GLU233**, LEU237, HIS299, **ASP300**, HIS305, ALA307

Molecular dynamics simulation (MDS)

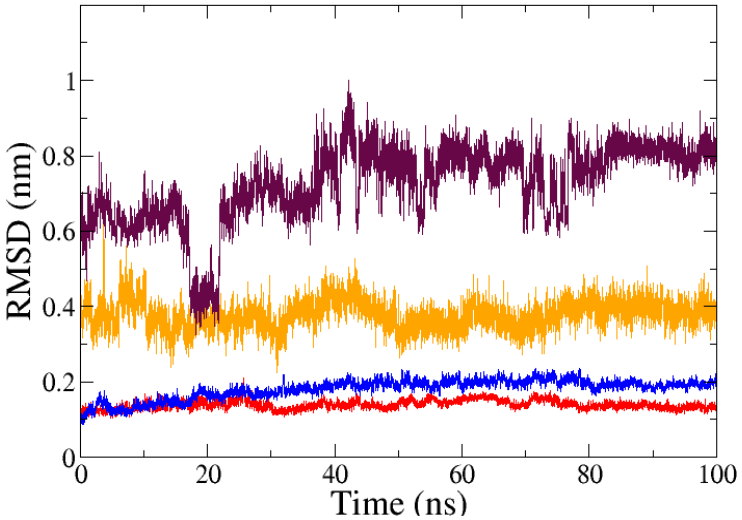

Fig. 5: RMSD of Rubuside F (orange) and Rubuside D (maroon) with respect to the protein backbone in Rubuside F complex and Rubuside D complex respectively; RMSD of protein backbone with respect to protein backbone in Rubuside F complex (red) and Rubuside D complex (blue).

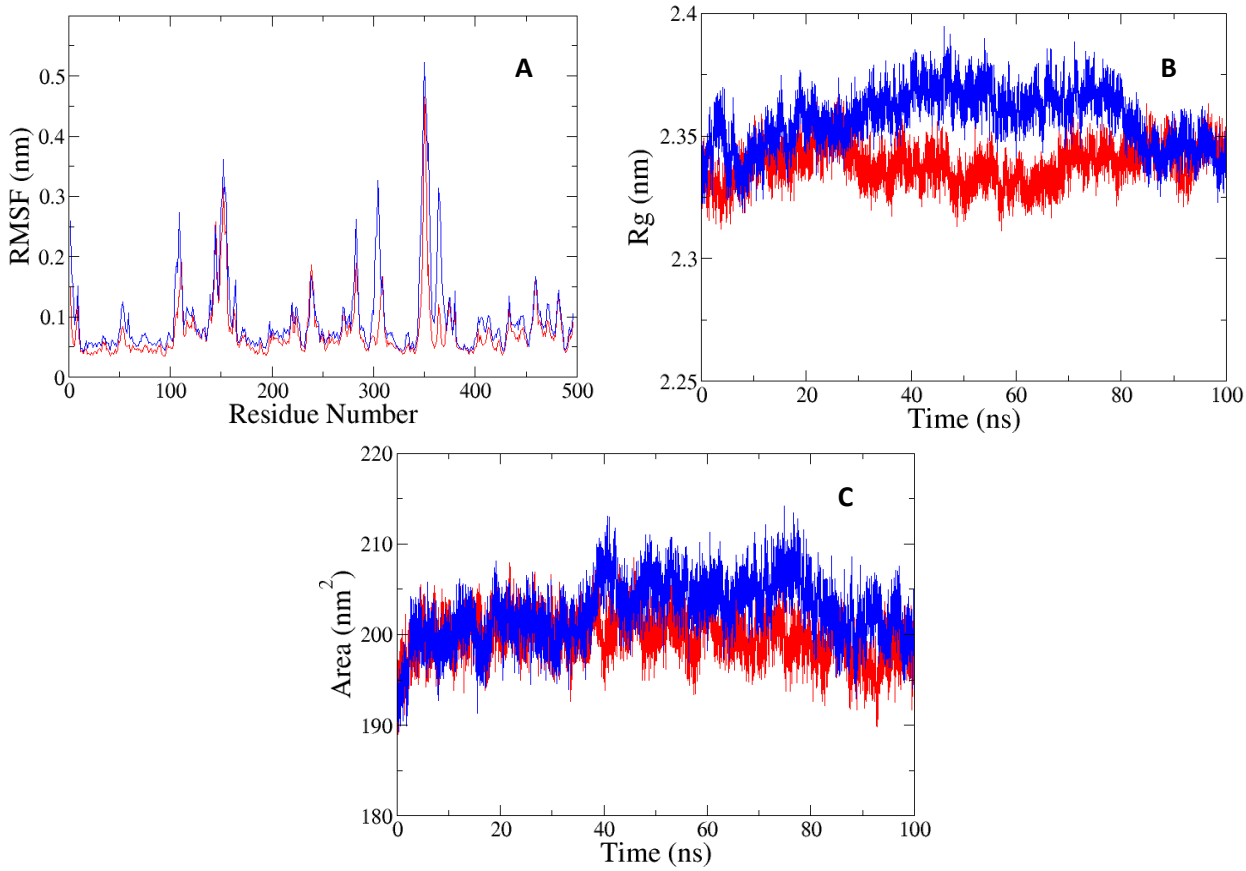

Fig. 6: (A) RMSF of α-carbon atoms, (B) Radius of gyration, and (C) SASA of protein in Rubuside F complex (red) and Rubuside D complex (blue).

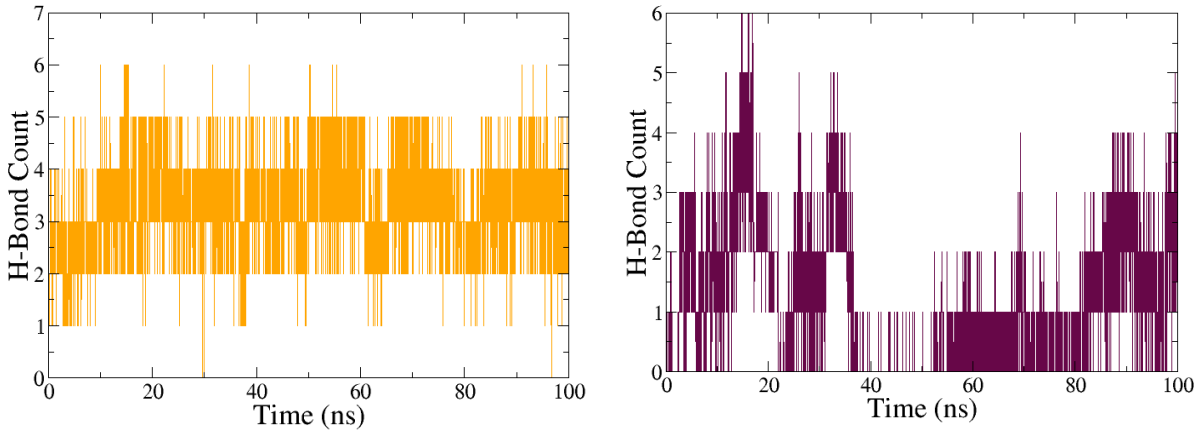

Fig. 7: Number of hydrogen bonds between ligands [Rubuside F (red), and Rubuside D (blue)] and human pancreatic α-amylase extracted from MDS trajectory.

The stability of the complex is evaluated through the RMSD profile obtained from the MD simulation and is shown in Figure 5 [41]. The lower the RMSD of the ligand, greater the stability of the protein-ligand system. From 100 ns MDS of the top two adducts from molecular docking, it was found that both the compounds showed geometrical stability with HPAA with an acceptable RMSD of ligand. Rubuside F showed greater stability with RMSD of ligand at around 4 *Å*. Rubuside D also exhibited stability of protein-ligand complex with an acceptable RMSD of 8 *Å*. Despite several spikes in MD trajectory, the ligand attained equilibrium with smooth curve for the last 20 ns of the simulation period.

The RMSF profile depicts the fluctuation of alpha-carbon atoms of the amino acid residues and is

shown in Figure 6A [42]. The spikes in RMSF plots of amino acid residues are possibly due to highly unstable fluctuating loop structures. The radii of gyration (R_g) of both the complexes were 23.5 *Å* and remained nearly constant with a stable trajectory suggesting no observable compression or expansion of the protein structure upon the ligand binding as shown in Figure 6B [43]. The solvent-accessible surface areas (SASA) were 200 nm^2 as depicted in Figure 6C and remained almost stable throughout the simulation period indicating no change in wettable area of the proteins upon the ligand binding [44].

The number of hydrogen bonds formed between the ligand and the protein molecule governs the stability of the adduct [45]. A higher number of hydrogen bonds were formed between rubuside F and the receptor. The number of hydrogen bonds frequently reached six and even seven a few times. In the case of rubuside D, fluctuation in the number of hydrogen bonds formed between the ligand and the protein was observed. Sporadically formed hydrogen bonds between 40 to 60 ns could have resulted in a slight rise in RMSD of the ligand as shown in Figure 5. Lower hydrogen bond count was observed in rubuside D than rubuside F which could have resulted in higher RMSD of rubuside D and lower RMSD of rubuside F as depicted in Figures 5 and 7.

Thus, the geometrical assessment through RMSD, RMSF, SASA, R_g and hydrogen bond count suggested that both the complexes were stable in nature and remained in the catalytic pocket throughout the production run. Therefore, it could possibly inhibit the normal functioning of human pancreatic α-amylase.

Binding Free energy calculation (MMPBSA)

Table 3: Change in binding free energy (kcal/mol) of complexes with it's various components for 20 ns from the MMPBSA method

Complex	$\Delta E_{VDWAALS}$	ΔE_{EL}	ΔE_{PB}	ΔE_{NPOLAR}	ΔG_{GAS}	ΔG_{SOLV}	ΔG_{BFE}
Rubuside F-amylase	-35.07± 3.01	-37.60± 6.03	49.36± 4.05	-4.61± 0.15	-72.67± 6.21	44.76± 4.01	-27.92± 4.15
Rubuside D-amylase	-39.28± 2.95	-23.56± 10.75	38.21± 8.16	-4.11± 0.15	-62.84± 10.59	34.09± 8.12	-28.75± 4.15

Spontaneity and feasibilty of the complex formation were evaluated through binding free energy change as shown in Table 3. Smaller the values of binding free energy changes (ΔG_{BFE}), the higher the thermodynamic stability of the complex [46]. Values less than zero ($\Delta G_{BFE}<0$) imply the spontaneity of the reaction. The binding free energy changes of -27.92±4.15 kcal/mol and -28.75±4.15 kcal/mol were estimated for rubuside F and rubuside D amylase complexes respectively. The negative value suggested that the complex formation was spontaneous in nature. Therefore, the compounds rubuside F and rubuside D could be potential inhibitors of HPAA.

CONCLUSION

Among the docked compounds, rubuside F and rubuside D showed highest binding affinity, geometrical stability with good RMSD of ligand and greater thermodynamical feasibility from binding free energy calculations. Both rubuside F and rubuside D could be proposed as potential inhibitors of human pancreatic α-amylase and thus could help in management of hyperglycemia and diabetes. Nevertheless, further in vitro and in vivo experiments are suggested to verify the computational results. Plants based drug candidates with efficacy could provide alternate therapeutics option for combating diabetes mellitus.

REFERENCE

[1] Holm, L.; Doll, J.; Holm, E.; Pancho, J. V.; & Herberger, J. P. World weeds:Natural histories and distribution, John Wiley & Sons (2017).

[2] Okigbo, R. N.; Eme, U. E.; & Ogbogu, S. Biodiversity and conservation of medicinal and aromatic plants in Africa. *Biotechnology and Molecular Biology Reviews*, **3**(6): 127-134 (2008).

[3] Cowan, M. Plant Products as Antimicrobial Agents. *Current Oncology*, **14**(4): 564–582 (1999).

[4] Kumar, A.; Singh, S. K.; Singh, V. K.; Kant, C.; Singh, A. K.; Tripathi, V.; Singh, K.; Sharma, V. K.; & Singh, J. An insight into the molecular docking interactions of plant secondary

metabolites with virulent factors causing common human diseases. *South African Journal of Botany*, **149**: 1008–1016 (2022).

[5] Vaou, N.; Stavropoulou, E.; Voidarou, C.; Tsigalou, C.; & Bezirtzoglou, E. Towards advances in medicinal plant antimicrobial activity: A review study on challenges and future perspectives. *Microorganisms*, **9**(10): 2041 (2021).

[6] Lamichhane, A.; Lamichhane, G.; & Devkota, H. P. Yellow Himalayan Raspberry (Rubus ellipticus Sm.): Ethnomedicinal, Nutraceutical, and Pharmacological Aspects. *Molecules*, **28**(16): 6071 (2023).

[7] Joshi, R. K.; Laurindo, L. F.; Rawat, P.; Goulart, R. de A.; & Barbalho, S. M. Himalayan Yellow Raspberry (Rubus ellipticus Smith.): A Plant with Multiple Medicinal Purposes. *Records of Agricultural and Food Chemistry*, **2**(2): 59–74 (2022).

[8] Wu, K.; Zhang, J.; Zhang, G.; & Ding, J. Epiblema tetragonana and Epinotia ustulana (Lepidoptera: Tortricidae), two potential biological control agents for the invasive plant, Rubus ellipticus. *Biological Control*, **77**: 51–58 (2014).

[9] Sharma, U. S.; & Kumar, A. Anti-diabetic effect of Rubus ellipticus fruit extracts in alloxan induced diabetic rats. *Journal of Diabetology*, **2**(2): 4 (2011).

[10] Vadivelan, R.; Bhadra, S.; Ravi, A.; Singh, K.; Shanish, A.; Elango, K.; & Suresh B. Evaluation of anti-inflammatory and membranestabilizing property of ethanol root extract ofRubus ellipticus Smith in Albino rats. *Journal of Natural Remedies*, **9**(1): 74–78 (2009).

[11] Jugran, A. K.; Rawat, S.; Devkota, H. P.; Bhatt, I. D.; & Rawal, R. S. Diabetes and plant-derived natural products: From ethnopharmacological approaches to their potential for modern drug discovery and development. *Phytotherapy Research*, **35**(1): 223-245 (2021). doi: 10.1002/ptr.6821.

[12] Sharma, S.; Kaur, R.; Kumar, K.; Kumar, D.; & Solanke, A. K. U. Genetic variability in Rubus ellipticus collections assessed by morphological traits and EST-SSR markers. *Journal of Plant Biochemistry and Biotechnology*, **30**(1): 37–55 (2021).

[13] Kaur, N.; Kumar, V.; Nayak, S. K.; Wadhwa, P.; Kaur, P.; & Sahu, S. K. Alpha- amylase as molecular target for treatment of diabetes mellitus: A comprehensive review. *Chemical Biology & Drug Design*, **98**(4): 539-560 (2021).

[14] Federation, I. D. *IDF Diabetes Atlas IDF Diabetes Atlas*. International Diabetes Federation (2021).

[15] Proença, C.; Freitas, M.; Ribeiro, D.; Tomé, S. M.; Oliveira, E. F. T.; Viegas, M. F.; Araújo, A. N.; Ramos, M. J.; Silva, A. M. S.; Fernandes, P. A.; & Fernandes, E. Evaluation of a flavonoids library for inhibition of pancreatic α-amylase towards a structure–activity relationship. *Journal of Enzyme Inhibition and Medicinal Chemistry*, **34**(1): 577–588 (2019).

[16] Basnet, S.; Ghimire, M. P.; Lamichhane, T. R.; Adhikari, R.; & Adhikari, A. Identification of potential human pancreatic α-amylase inhibitors from natural products by molecular docking, MM/GBSA calculations, MD simulations, and ADMET analysis. *Plos One*, **18**(0275765) (2023).

[17] Etsassala, N. G. E. R.; Badmus, J. A.; Marnewick, J. L.; Iwuoha, E. I.; Nchu, F.; & Hussein, A. A. Alpha-glucosidase and alpha-amylase inhibitory activities, molecular docking, and antioxidant capacities of salvia aurita constituents. *Antioxidants*, **9**(11): 1–14 (2020).

[18] Jacob, B.; & Narendhirakannan, R. T. Role of medicinal plants in the management of diabetes mellitus: a review. *3 Biotech*, **9**: 1-17 (2019).

[19] Huang, S. Y.; & Zou, X. Advances and challenges in protein-ligand docking. *International Journal of Molecular Sciences*, **11**(8): 3016-3034 (2010).

[20] Li, W.; Fu, H.; Bai, H.; Sasaki, T.; Kato, H.; & Koike, K. Triterpenoid saponins from Rubus ellipticus var. obcordatus. *Journal of Natural Products*, **72**(10): 1755–1760 (2009).

[21] Prakash, V.; Kumari, A.; Kaur, H.; Kumar, M.; Gupta, S., Bala, R.; & Gupta, D. Traditional Medicinal Values of Rubus ellipticus with Biological Activities Observed from its Crude Extract: A Review. *Ecology, Environment and Conservation*, **28**: 217–226 (2022).

[22] Kewlani, P.; Singh, L.; Belwal, T.; & Bhatt, I. D. Optimization of ultrasonic-assisted extraction for bioactive compounds in Rubus ellipticus fruits: An important source for nutraceutical and functional foods. *Sustainable Chemistry and Pharmacy*, **25**: 100603 (2022).

[23] Kewlani, P.; Tiwari, D.; Rawat, S.; & Bhatt, I. D. Pharmacological and phytochemical potential of Rubus ellipticus: a wild edible with multiple health benefits. *Journal of Pharmacy and Pharmacology*, **75**(2): 143-161 (2023).

[24] Li, Z.; Wan, H.; Shi, Y.; & Ouyang, P. Personal experience with four kinds of chemical structure drawing software: review on ChemDraw, ChemWindow, ISIS/Draw, and ChemSketch. *Journal of Chemical Information and Computer Sciences*, **44**(5): 1886-1890 (2004).

[25] Trott, O.; & Olson, A. J. AutoDock Vina: Improving the speed and accuracy of docking with a new scoring function, efficient

optimization, and multithreading. *Journal of Computational Chemistry*, **31**(2): 455-461 (2009).

[26] Hanwell, M. D.; Curtis, D. E.; Lonie, D. C.; Vandermeersch, T.; Zurek, E.; & Hutchison, G. R. Avogadro: an advanced semantic chemical editor, visualization, and analysis platform. *Journal of Cheminformatics*, **4**(8): 1-17 (2012).

[27] Berman, H. M.; Westbrook, J.; Feng, Z.; Gilliland, G.; Bhat, T. N.; Weissig, H.; Shindyalov, I. N.; & Bourne, P. E. The protein data bank. *Nucleic Acids Research*, **28**(1): 235-242 (2000).

[28] Yuan, S.; Chan, H. S.; & Hu, Z. Using PyMOL as a platform for computational drug design. *Wiley Interdisciplinary Reviews: Computational Molecular Science*, **7**(2) (2017).

[29] Kitchen, D. B.; Decornez, H.; Furr, J. R.; & Bajorath, J. Docking and scoring in virtual screening for drug discovery: methods and applications. *Nature Reviews Drug discovery*, **3**(11): 935-949 (2004).

[30] Systèmes, D. BIOVIA Discovery Studio *Dassault Syst mes BIOVIA, Discovery Studio Modeling Environment, Release 202* (2021).

[31] Pettersen, E. F.; Goddard, T. D.; Huang, C. C.; Couch, G. S.; Greenblatt, D. M.; Meng, E. C.; & Ferrin, T. E. UCSF Chimera - A visualization system for exploratory research and analysis. *Journal of Computational Chemistry*, **25**(13): 1605–1612 (2004).

[32] Ramírez, D.; & Caballero, J. Is it reliable to take the molecular docking top scoring position as the best solution without considering available structural data?. *Molecules*, **23**(5): 1038 (2018).

[33] Abraham, M. J.; Murtola, T.; Schulz, R.; Páll, S.; Smith, J. C.; Hess, B.; & Lindah, E. Gromacs: High performance molecular simulations through multi-level parallelism from laptops to supercomputers. *SoftwareX*, **1**: 19–25 (2015).

[34] Foloppe, N.; & MacKerell, A. D. All-atom empirical force field for nucleic acids: I. Parameter optimization based on small molecule and condensed phase macromolecular target data. *Journal of Computational Chemistry*, **21**(2): 86-104 (2000).

[35] Zoete, V.; Cuendet, M. A.; Grosdidier, A.; & Michielin, O. SwissParam: A fast force field generation tool for small organic molecules. *Journal of Computational Chemistry*, **32**(11): 2359–2368 (2011).

[36] Valdés-Tresanco, M. S.; Valdés-Tresanco, M. E.; Valiente, P. A.; & Moreno, E. Gmx_MMPBSA: A New Tool to Perform End-State Free Energy Calculations with GROMACS. *Journal of Chemical Theory and Computation*, **17**(10): 6281–6291 (2021).

[37] Dong, L.; Qu, X.; Zhao, Y.; & Wang, B. Prediction of Binding Free Energy of Protein-Ligand Complexes with a Hybrid Molecular Mechanics/Generalized Born Surface Area and Machine Learning Method. *ACS Omega*, **6**(48): 32938–32947 (2021).

[38] Pantsar, T.; & Poso, A. Binding affinity via docking: fact and fiction. *Molecules*, **23**(8): 1899 (2018).

[39] Erickson, J. A., Jalaie, M., Robertson, D. H., Lewis, R. A., & Vieth, M.. Lessons in Molecular Recognition: The Effects of Ligand and Protein Flexibility on Molecular Docking Accuracy. *Journal of Medicinal Chemistry*, **47**(1): 45–55 (2004).

[40] Torres, P. H.; Sodero, A. C.; Jofily, P.; & Silva-Jr, F. P. Key topics in molecular docking for drug design. *International Journal of Molecular Sciences*, **20**(18): 4574 (2019).

[41] Adcock, S. A.; & McCammon, J. A. Molecular dynamics: survey of methods for simulating the activity of proteins. *Chemical Reviews*, **106**(5): 1589-1615 (2006).

[42] Martínez, L. Automatic identification of mobile and rigid substructures in molecular dynamics simulations and fractional structural fluctuation analysis. *PLoS ONE*, **10**(0119264) (2015).

[43] Lobanov, M. Y.; Bogatyreva, N. S.; & Galzitskaya, O. V. Radius of gyration as an indicator of protein structure compactness. *Molecular Biology*, **42**(4): 623–628 (2008).

[44] Durham, E.; Dorr, B.; Woetzel, N.; Staritzbichler, R.; & Meiler, J. Solvent accessible surface area approximations for rapid and accurate protein structure prediction. *Journal of Molecular Modeling*, **15**(9): 1093–1108 (2009).

[45] Chikalov, I.; Yao, P.; Moshkov, M.; & Latombe, J. C. Learning probabilistic models of hydrogen bond stability from molecular dynamics simulation trajectories. *BMC Bioinformatics*, **12**(1): 1-6 (2011).

[46] Perozzo, R.; Folkers, G.; & Scapozza, L. Thermodynamics of protein–ligand interactions: history, presence, and future aspects. *Journal of Receptors and Signal Transduction*, **24**(1-2): 1-52 (2004).